Arch. Metall. Mater. **64** (2019), 4, 1617-1625

DOI: 10.24425/amm.2019.130135

P. FIGIEL*#, A. BIEDUNKIEWICZ*, W. BIEDUNKIEWICZ**, D. GRZESIAK**, M. PAWLYTA***

CORROSION CHARACTERISTICS OF COMPOSITES OF (Mo,Ti)C/Ti AND TiC/Ti TYPE MANUFACTURED WITH SLM TECHNIQUE

The addition of hard ceramic particles of nc-(Ti,Mo)C in carbon network into Ti matrix has been proved to be an efficient way to enhance their properties. The purpose of this work was to analyze the corrosion, tribological, mechanical and morphological effects of combining nc-(Ti,Mo)C/C with titanium metal, to create a unique composite via selective laser melting technique (SLM). Composites with different weight percentage (5, 10 and 20 wt %) of ceramic phase were produced. The samples of pure Ti and Ti-6Al-4V alloy were also tested, as a reference. These composites were examined for corrosion resistance in body fluid (artificial saliva solution). Moreover, the properties of titanium composites reinforced with nc-TiC powders were compared. It was stated that mechanical properties were significantly improved with increasing amount of nc-(Ti,Mo)C/C in Ti matrix. In terms of corrosion resistance, the composites showed worse properties compared to pure titanium and Ti-6Al-4V alloy, but better than TiC-reinforced composites.

Keywords: Nanocomposites, TiMCs, SLM, (Ti,Mo)C

1. Introduction

Long-term performance of surgical implants is often restricted by their surface properties. Titanium is found to be well tolerated and nearly an inert material in the human body environment. In an optimal situation titanium is capable of osseointegration with bone [1,2]. Titanium forms a very stable passive layer of TiO_2 on its surface and provides superior corrosion resistance and biocompatibility. Even if the passive layer is damaged, the layer is immediately rebuilt. Moreover, titanium alloy implants produce corrosion particles and fail by mechanisms generally related to surface interaction on bone to promote an inflammation with fibrous aseptic loosening or infection that can require implant removal [3]. Commercially pure titanium (cp-Ti) is less expensive, generally more corrosion resistant and lower in strength than its alloys. Low modulus of elasticity of the titanium means excellent flexibility and strong spring back characteristics. This promotes its use in various springs for aircraft and valves, where a modulus half that of steel, but a strength equivalent to steel allows a titanium spring to be half as large and heavy. The use of Ti and its alloys as construction materials under severe friction and wear conditions is limited due to their poor tribological properties [4-6]. The mechanical, thermo-mechanical and wear properties of titanium metal can be improved by reinforcing them with ceramics [7-10]. There is considerable interest in the development of Ti-based Metal Matrix Composites (TiMMCs) reinforced with high-stiffness ceramic reinforcements. While offering an elevated-temperature resistant, ductile base, titanium can be further strengthened with the addition of ceramic compounds in fiber or particulate form to produce properties beyond those achieved by alloying alone. Various combinations of useful properties, usually not attainable by alloys, can be obtained through composite materials by suitable tailoring the matrix and reinforcement. Generally, metal matrix composites are used in wear applications, due to their high hardness while maintaining a reasonable level of toughness [11]. Wear resistance is one key aspect where the intrinsic properties of MMCs may be exploited.

In order to maximize interfacial bond strength in Metal Matrix Composites (MMCs), it is necessary to promote wetting, control chemical interactions and minimize oxide formation. The interfacial connection (consolidation of the composite) is possible through the chemical reaction between the matrix and the strengthening phase taking place in the sintering process. This approach guarantees a thermodynamically stable composite with clean interphase surfaces, well-consolidated, with maximum strength at low and elevated temperatures and fracture toughness.

Decreasing the ceramic particle size can lead to a substantial improvement in mechanical properties of Titanium Matrix Composites (TMCs), e.g., enhanced strengthening and reduced

* WEST POMERANIAN UNIVERSITY OF TECHNOLOGY, FACULTY OF MECHANICAL ENGINEERING AND MECHATRONICS, 19 PIASTOW AV., 70-310 SZCZECIN, POLAND
** WEST POMERANIAN UNIVERSITY OF TECHNOLOGY, FACULTY OF MECHANICAL ENGINEERING AND MECHATRONICS, INSTITUTE OF MANUFACTURING ENGINEERING, 19 PIASTOW AV., 70-310 SZCZECIN, POLAND
*** SILESIAN UNIVERSITY OF TECHNOLOGY, FACULTY OF MECHANICAL ENGINEERING, KONARSKIEGO 18A, 44-100 GLIWICE, POLAND
# Corresponding author: pfigiel@zut.edu.pl

particle cracking [12-14]. In addition, the dispersion of the ceramic phase at the nanoscale with controlled nanostructures in TMC tends to introduce new behaviors that are not found in unreinforced titanium [15].

In the binary Ti-C system cubic-TiC (B1, Fm_3m) is a typical representative of an interstitial transition metal carbide. Similarly to most carbides, the structure can accommodate a large concentration of defects on the "interstitial" carbon positions, leading to substoichiometric TiC_{1-x}, with $0.535 < x < 0.023$. The binary Mo-C system has several phases most of which have two compositions, MoC and Mo_2C. The stoichiometric fcc-MoC phase, which crystallizes in a NaCl-type structure (B1-type) is metastable [16]. Important features such as the carbon non-stoichiometry and a possible ordered structure for the carbon vacancies still remain unexplained up to date. Corresponding to authors [17] the vacancies are ordered in long range in the host structure, a thermodynamically-stable structure with ordered vacancies did not account for the robust features of δ-$MoC_{0.681}$. Instead, the inherent phonon instability, theoretically predicted for the stoichiometric MoC, might be responsible for the robust carbon vacancies of δ-$MoC_{0.681}$. The isomorphous carbides TiC and MoC_{1-x} form a continuous series of solid solutions at high temperatures. Stabilization of cubic MoC can be also achieved by replacing a small amount of Mo atoms by Ti atoms together with the formation of carbon vacancies. It is found that stable $Mo_xTi_{1-x}C_y$ cubic carbide can be formed only at sufficiently great amount of Ti atoms ($x < 0.2$) [18]. The role of Mo partly substitutes for Ti in the TiC lattice was investigated by Jang et al. [19]. It has been reported that the coarsening kinetics of TiC particles can be controlled using molybdenum additions [20]. The lattice parameter for MoC determined by preserving the phases by rapid quenching in order to suppress their hexagonal form with the M_2C formula unit, has been reported as $a_{MoC} = 4.28$ Å [21]. This parameter is smaller than that of TiC. Supposing lattice parameters of $a_{Ti\alpha} = 2.95$ Å and $a_{TiC} = 4.32$ Å, the lattice fit between Ti_α and TiC is insufficient. Small lattice misfit suggests that coherent interfaces could be possible. This means that a contraction of the TiC lattice is necessary to maintain the coherency at the interface with the Ti_α matrix. It should be recognized that Mo addition can mitigate the lattice mismatch between the carbide particle and the titanium alfa matrix. Meeting the requirements, i.e. adequate bonding between matrix and particles, coherent interfaces, decreasing the ceramic particle size, the dispersion of the ceramic phase, can affect the beneficial properties of the TMCs such as strength, creep resistance, intergranular corrosion resistance.

In this work, the incremental technique of selective laser melting was used for the titanium composite manufacturing process. SLM builds parts in a layer-by-layer manner by selectively fusing and consolidating thin layers of loose powder using a high-energy laser beam. The purpose of this investigation was to understand the corrosion, mechanical and morphological effects of combining titanium carbide with titanium metal to create a unique composite via SLM. The properties of titanium composites reinforced with nanocrystalline (Ti,Mo)C/C and TiC/C powders were compared. The effect of the presence of carbon cages on the surface of nanoparticles in the consolidation process of these carbides and Ti matrix on the properties of the Titanium Metal Matrix NanoComposites (TiMMNCs) was also analyzed. The tests were carried out for cp-Ti and Ti-6Al-4V alloy samples prepared using the same method and under the same conditions as in the case of composites.

2. Materials and methods

2.1. Preparation of Ti/TiC composites

The one type of cp-Ti (grade 1), obtained by gas atomization from SLM Solutions GmbH, was employed as starting matrix material. Cp-Ti had a spherical shape and its average particle size was around 100 μm (Fig. 1a). As a reinforcements (Ti,Mo)C nanoparticles (NPs) embedded in carbon network with an average crystallite size of 12 nm and ca 40 wt % elemental carbon content (designated as nc-(Ti,Mo)C/C) (Fig. 1b) were used. The molar ratio of Ti/Mo was equal 10:1. In order to assess the effect of molybdenum, samples of titanium composites were prepared, in which the nanocrystalline titanium carbide embedded in carbon network (TiC/C) was used as a reinforcement phase with an average crystallite size of 40 nm and ca 3 wt % elemental carbon

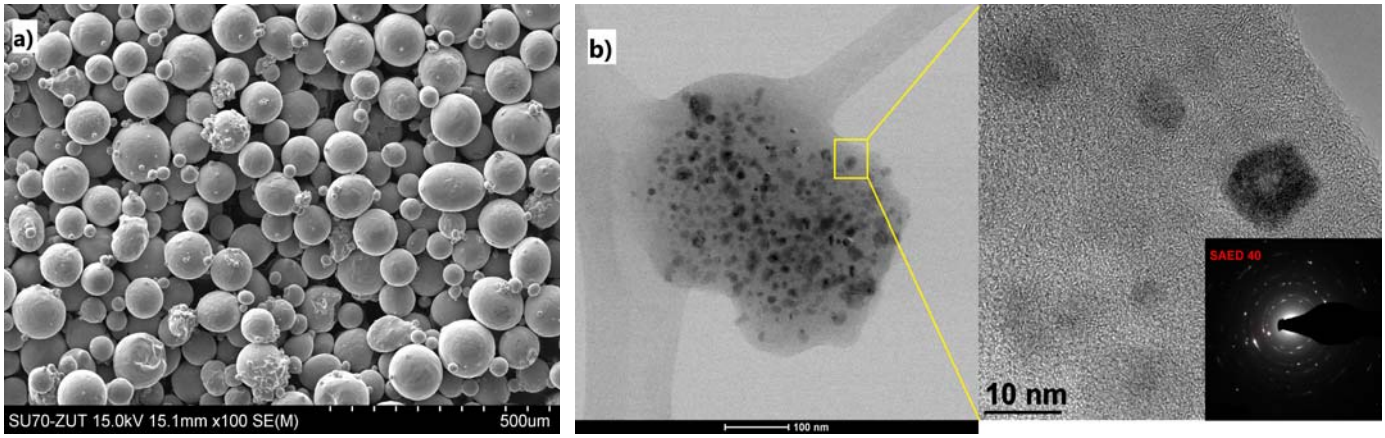

Fig. 1. Morphology of starting material: a) SEM image of cp-Ti powder, b) TEM image of nc-(Ti,Mo)C/C powders and corresponding SAED pattern

content (designated as nc-TiC/C). Nanocrystalline carbides of the type (Ti,Mo)C/C and TiC/C were obtained by a nonhydrolytic sol-gel method [22].

The Ti with the (Ti,Mo)C/C or TiC/C powders were milled in argon atmosphere using a planetary mill Pulverisette 4 (Fritsch GmbH), with use of the WC/Co milling balls in a weight ratio of 10:1 with respect to the powder. For sintering process the mixtures of the powders composed of 0, 5, 10, and 20 wt % of (Ti,Mo)C/C and the titanium were used.

Selective Laser Melting technique (SLM) was used to study the effect of the size and presence of carbon cages on the surface of TiC particles distributed in titanium matrix in the consolidation process of (Ti,Mo)C and Ti on the properties of the TiMMCs. The SLM system (MCP HEK Realizer II) consisted of Nd:YAG fiber laser, an automated powder layer feeder and argon gas protection system to avoid material oxidation. A powder layer thickness (d) of 50 μm, hatch distance (h) of 50 μm, laser power of 100 W and scan speed of 300 mm/s were applied. The value of volumetric energy density (η), calculated on the basis of these parameters was 133 J/mm^3. The samples obtained in the process had cylindrical shape with a diameter of 15 mm and a height of 4 mm. For comparison the samples of the alloy of Ti-6Al-4V and cp-Ti were prepared using the same method and under the same conditions as in the case of the composites. To prepare samples of the cp-Ti and Ti-6Al-4V alloy, commercial SLM Solutions GmbH powders were used. All the examinations were performed on the surface perpendicular to the direction of growth/build of the composite.

2.2. Structural characterization

Samples for XRD examination and corrosion characterization were cut, then ground and polished using an ATM SAPHIR 550 grinder with a MD-Mezzo 220 disk and MD-Largo discs with the addition of 9 μm diamond suspension. Finishing step was carried out on MD-Chem disks using Al_2O_3 suspension with the addition of H_2O_2. For morphology investigation the second group of samples was grinded with 220 grit paper and electro-polished with Struers LectoPol-5 device, with the following parameters: 30-35V voltage, 20s time, 1 cm^2 surface and Struers A3 electrolyte.

The average size of crystallites in composites was estimated applying Scherrer's formula. The size of crystallites, phase composition of the composites was determined based on X-Ray diffraction (XRD) using PANalytical PW3040/60 X'Pert Pro apparatus equipped with Cu Kα radiation.

The FEI Titan G2 80-300 TEM / STEM microscope equipped with EDS energy dispersive X-ray spectrometer was used to analyze the structure and morphology of the composites. The lamellas were prepared on SEM/Ga-FIB FEI Helios Nanolab^{TM} 600i apparatus. Samples were cut in a direction parallel to the direction of composite growth, i.e. perpendicular to the surface analyzed by XRD. The lamella was cleaned using a plasma cleaner.

2.3. Mechanical and corrosion tests

The Vickers hardness, HV, measurements were performed on Leco LM247AT indenter applying a 100 g load with an indentation time of 10s. Average hardness values of at least 10 measurements per sample were determined. Standard deviations did not exceed 10%.

In order to investigate coefficient of friction (COF) of the composites ball-on-disk method was applied. The tests were performed under ambient dry conditions on CSM tribometer (TRN model). Alumina ball with the diameter of 6 mm was slid on disc made of tested materials in rotating mode. The applied load was 5 N, and sliding distance was 500 m. Before each test, the specimens and balls were rinsed ultrasonically in acetone.

Open-circuit corrosion potential (OCP) measurements were carried out in the separate cell for 24 hours while potentiodynamic polarization measurements were performed using a scan rate of 1 mV/s at a potential initiated at −1.5 V to +2.5 V. The measurement was carried out on the Atlas-Sollich 9833 potentiostat in a three-electrode system. The calomel (reference) and graphite (auxiliary) electrodes were used. The analysis of the results has been carried out by means of the AtlasLab software. Corrosion parameters were calculated from Tafel slops. All corrosion tests were carried out in artificial saliva fluids at 37°C with a pH of 6.7. The composition of artificial saliva is given in Table 1.

TABLE 1

Chemical composition of Fusayama-Meyer artificial saliva solution in H_2O; pH = 6.7

Reagent	Quantity, [g/dm^3]
$(NH_2)_2CO$	1.0
NaCl	0.4
KCl	0.4
$CaCl_2$ $2H_2O$	0.795
NaH_2PO_4	0.69
Na_2S $9H_2O$	0.005
KSCN	0.3

3. Results and discussion

The X-ray diffraction patterns are used to analyze the phase composition of the samples and are shown in Figures 2, 3 and 4. Figure 2 shows X-ray diffraction pattern of the carbide phase of (Ti,Mo)C type embedded in carbon network. The broad peak at 25.39° can be attributed to carbon (002), and the other six sharp peaks at 36.335° (111), 42.188° (200), 61.198° (220), 73.282° (311) and 77.168° (222) and 92.021 (004) can be well assigned to (Ti,Mo)C [23]. Figure 3 shows X-ray diffraction patterns of the cp-Ti and Ti-6Al-4V alloy powder after SLM process. The example of XRD patterns of the titanium matrix composites containing respectively 5, 10, and 20 wt % of (Ti,Mo)C/C and 5, and 10 wt % of TiC/C are presented in Figure 4.

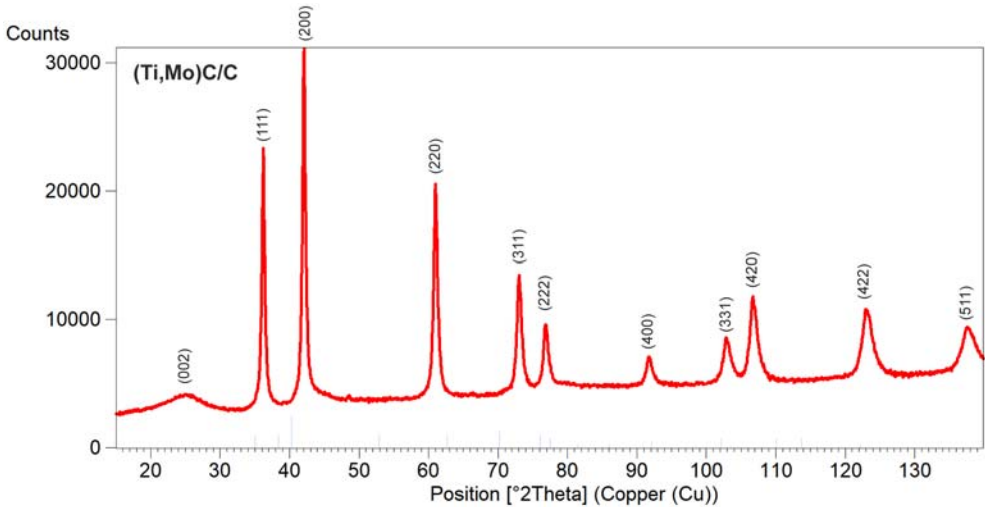

Fig. 2. X-ray diffraction pattern of the carbide phase of (Ti,Mo)C type in the carbon cages

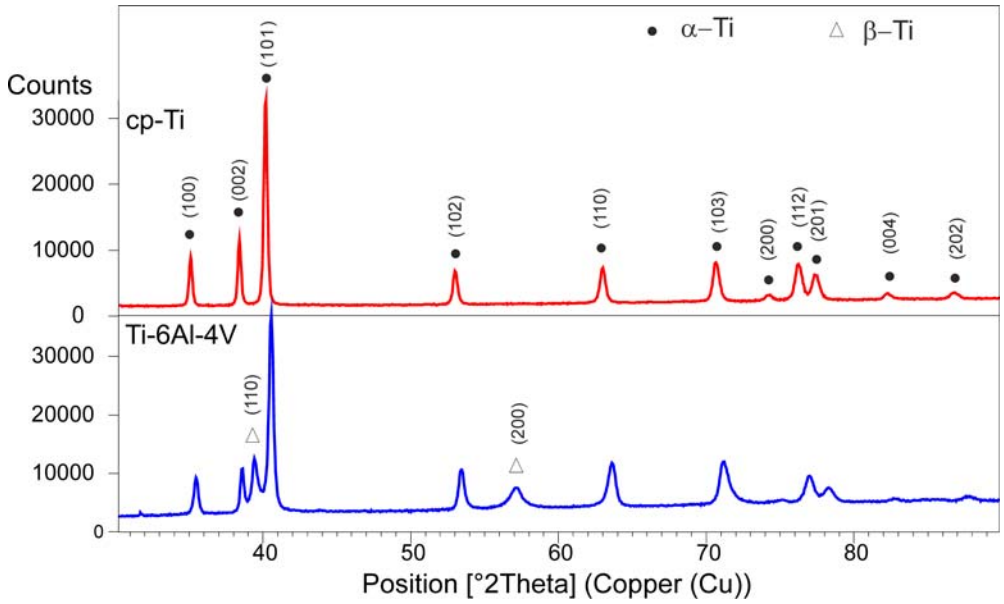

Fig. 3. X-ray diffraction patterns of the cp-Ti and Ti-6Al-4V alloy samples prepared via SLM technique

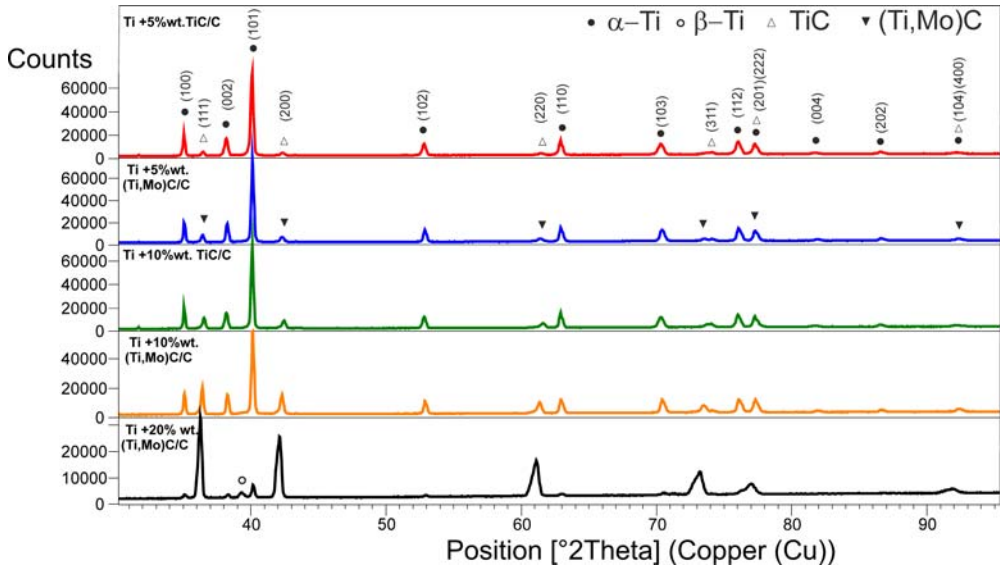

Fig. 4. Comparison of the X-ray diffraction patterns of the (Ti,Mo)C/Ti composites after SLM process

Analyzing the results of X-ray diffraction tests, there is observed a change in the intensity distribution of interference reflections of the titanium matrix with the increase in the content of titanium carbide in the composites. The I_{101}/I_{002} of Ti peak's ratio in composite samples are not the same as the data in JCPDS card. With the increase of the mass fraction of (Ti,Mo)C/C in the titanium matrix, the I_{101}/I_{002} of Ti peak's ratio in composite samples increases. This ratio increases from 3.8 by 3.84, 4.24 and 4.46 respectively for 0, 5, 10 and 20 wt % of (Ti,Mo)C/C in the titanium matrix. The I_{101}/I_{002} of Ti peak's ratio is equal 3.85 for the most closely matched Ti standard in the ICDD file (card number 00-005-0682). This indicates that in some of composite samples Ti phase exhibits some texture. The increase of the strengthening phase is involved in the reorientation of titanium crystallites from random to anisotropic. In the case of TiC/Ti composites a similar reorientation of Ti crystallites was observed along with an increase of the nc-TiC/C weight fraction. The I_{101}/I_{002} of Ti peak's ratio increases from 3.8 by 3.87, 4.15 respectively for 0, 5, 10 wt % of TiC/C in the titanium matrix.

In addition, there was a change in the distribution of the intensity of lines of interference strengthening phases in the titanium matrix. In the tested titanium composites, both TiC crystals and (Ti,Mo)C exhibited a texture. In all the examined composites, a higher intensity of the d_{111} diffraction line was observed compared to the d_{200} line, which indicates the texture of carbides of (Ti,Mo)C and TiC type in the titanium matrix. The I_{200}/I_{111} of (Ti,Mo)C peak's ratio increases from 0.899 to 0.928 as the weight fraction of (Ti,Mo)C increases from 5 to 10 wt % in the titanium matrix. In the case of a composite with a content of 20 wt% (Ti,Mo)C/C, the analysis of the line profile (111) and (200) allows the identification of two sub-networks, probably TiC and (Ti,Mo)C, to which the I_{200}/I_{111} of the carbide peak's ratio was assigned with values of 2.092 and 0.539, respectively. The I_{200}/I_{111} of (Ti,Mo)C peak's ratio in the case of pure (Ti,Mo)C/C powder is 1.623. The I_{200}/I_{111} of TiC peak's ratio increases from 0.859 to 0.866 respectively for 5 and 10 wt % of TiC/C in the titanium matrix. The I_{200}/I_{111} of TiC peak's ratio in the case of pure TiC/C powder is 1.618.

During the sintering/melting step in SLM process, the metallic phase forms a liquid in which dissolution and transport of the carbide mass took place. Under such conditions the reaction between titanium and elemental carbon occurred. Comparison of the intensities of interference reflections of carbides and titanium of the matrix, shows that the titanium matrix quantitatively dominates in composites with 5 and 10 wt % of (Ti,Mo)C and also TiC, while in 20 wt % of (Ti,Mo)C composite, the carbides quantitatively prevail in comparison to the metal matrix phases. The amount of 40 wt. % of free carbon in (Ti,Mo)C/C powder, causes loss of titanium in the matrix during the consolidation process. This loss is multiplied by the proportion of the powder introduced in the strengthening phase according to the reaction:

$$Ti + C = TiC \quad (1)$$

Additionally, the increase of titanium carbide may be caused carbothermal reduction of TiO_2 (passive layer on Ti powder) in the following reaction:

$$TiO_2 + 2C = TiC + CO_2 \quad (2)$$

There is also a decomposition of the (Ti,Mo)C type carbide with the possibility of creating core-rim structures due to diffusion of molybdenum towards the titanium matrix. The (Ti,Mo)C type carbide decomposes into two phases with different Mo content and the TiC cores might be regarded as a stable phase. The rim phase is (Ti,Mo)C solid solution. Therefore, it is possible to create carbides with different Mo content and molybdenum depletion in its core. The core-rim structure was predicted to be thermodynamically unstable in the Ti-Mo-C system [24]. It is believed that the core-rim structure is actually beneficial because of the kinetic cause. The structure of the tested composite of (Ti,Mo)C/Ti type may contain carbides slightly differing in the parameters of the crystal lattice. This was clearly observed on the diffractogram of a composite containing 20 wt % of (Ti,Mo)C/C. This phenomenon is illustrated by the peak profile analysis in the figure 5.

SEM and TEM images of the microstructure of the (Ti,Mo)C/Ti composites illustrated in figures 6÷9 give evidence for the

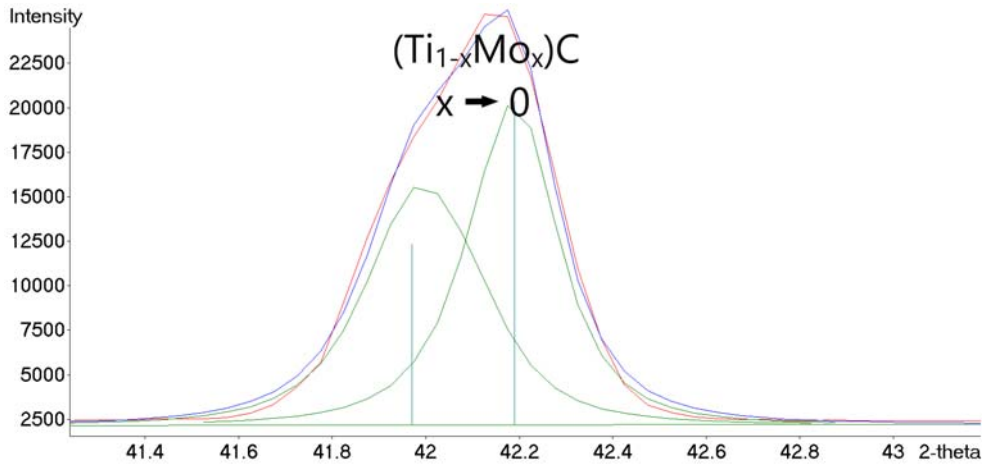

Fig. 5. Decomposition of (200) diffraction peak of (Ti,Mo)C

distribution of reinforcements in the matrix. These observations showed that the strengthening phase consisted of nanostructured grains with a few micrometer size (Fig. 8), which included crystallites of a size of several nanometers (Fig. 9).

The graph in Figure 10 demonstrates the values of hardness with respect to reinforcing quantity of (Ti,Mo)C/C. The results showed that the hardness increased with increasing carbide content. Table 2 presents the values of coefficients of friction of (Ti,Mo)C/Ti composites and cp-Ti and Ti-6Al-4V alloy. The composites were characterized by slightly higher values of COF in comparison to cp-Ti and Ti-6Al-4V alloy.

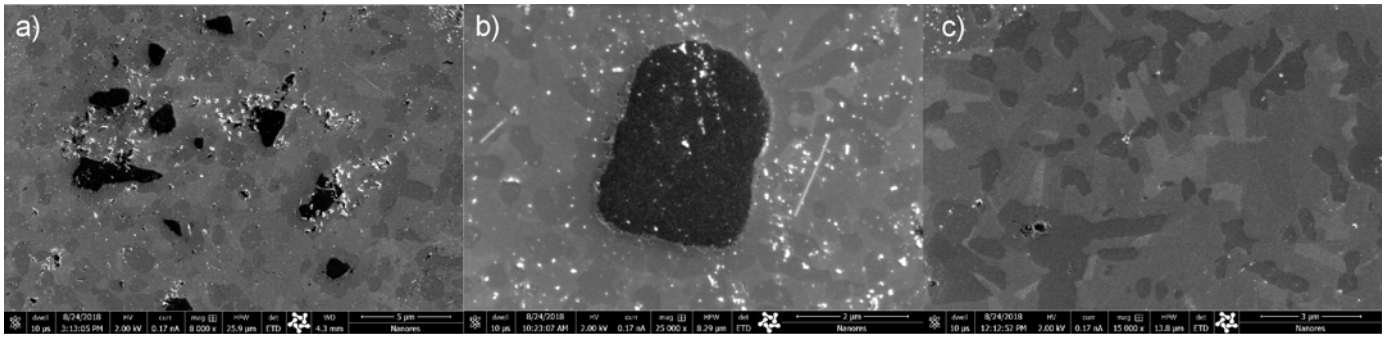

Fig. 6. SEM images of the microstructure of the titanium composite containing 10 wt. % of (Ti,Mo)C/C – the surface perpendicular to the direction of growth, a) general view, b) carbide image, c) image of the surroundings matrix

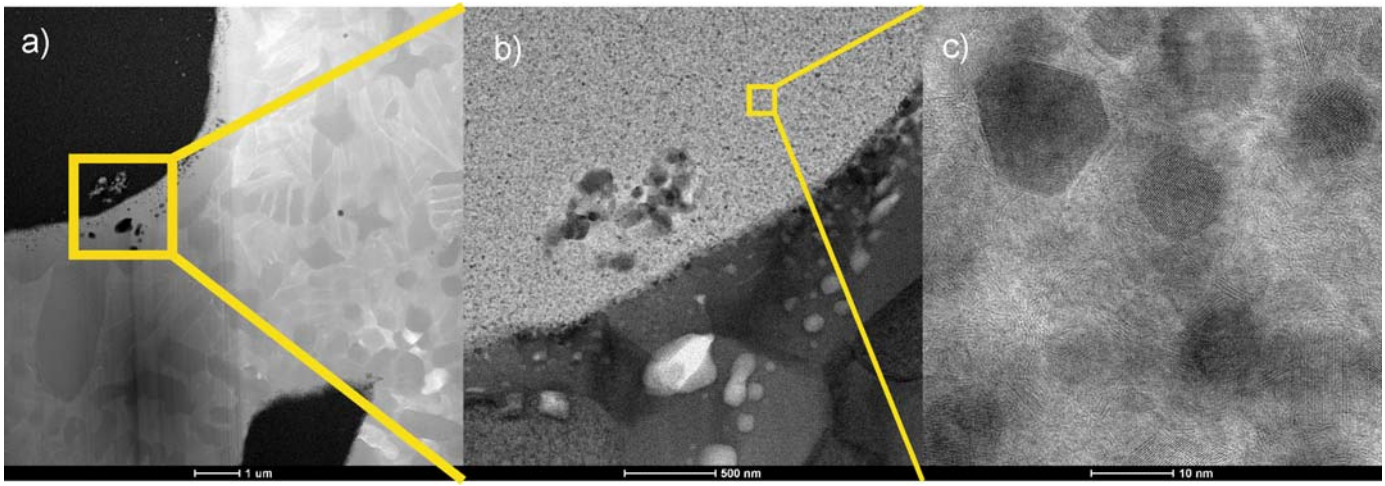

Fig. 7. Microstructure of the titanium composite containing 10 wt. % of (Ti,Mo)C/C (the lamella) – surface perpendicular to the direction of composite growth, a i b) TEM images of the composite obtained on BF and HAADF detectors, c) high-resolution TEM image of (Ti,Mo)C phase

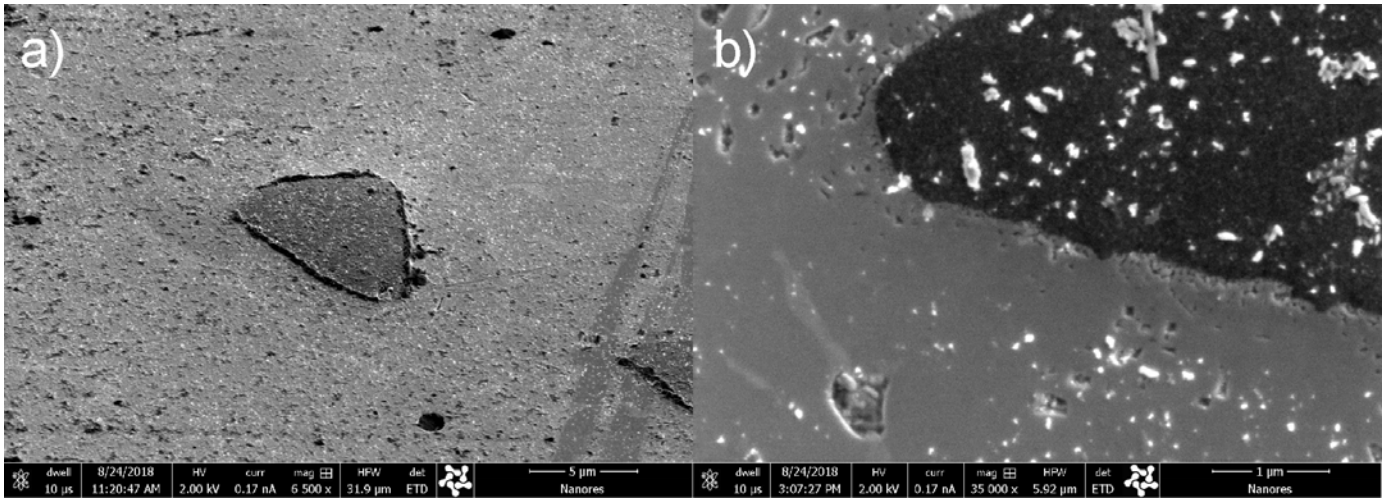

Fig. 8. SEM image of the microstructure of the titanium composite containing 20 wt. % of (Ti,Mo)C/C – the surface perpendicular to the direction of growth, a) general view, b) carbide and surroundings matrix

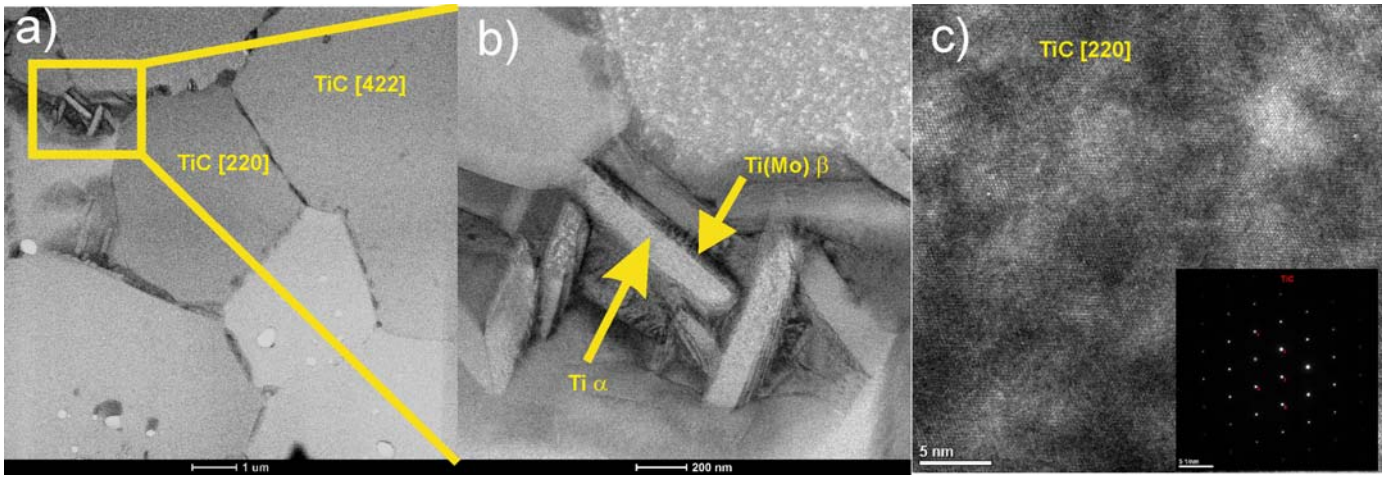

Fig. 9. TEM morphology of (Ti,Mo)C/Ti composites containing 20 wt. % of (Ti,Mo)C/C, a,b) TEM image of (Ti,Mo)C/Ti composites obtained on BF detector, c) high-resolution TEM image of TiC [220] phase with corresponding SEAD pattern

TABLE 2

Comparison of average values of friction coefficients

Samples	Average coefficient of friction	Standard deviation
cp-Ti	0.670	0.031
Ti-6Al-4V	0.528	0.019
Ti + 5 wt % (Ti,Mo)C	0.734	0.039
Ti + 10 wt % (Ti,Mo)C	0.766	0.083
Ti + 20 wt % (Ti,Mo)C	0.734	0.044

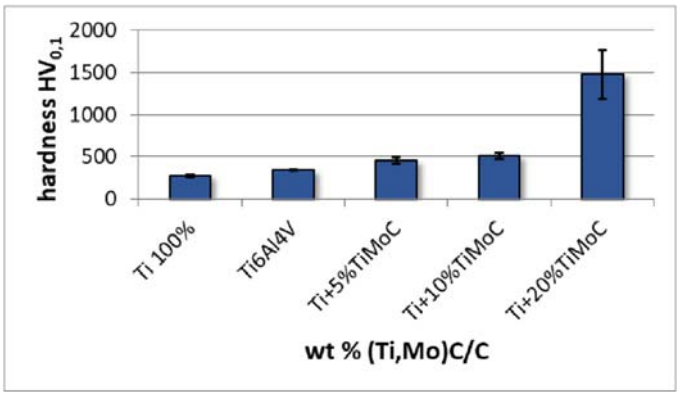

Fig. 10. Hardness of the composites with respect to reinforcing quantity of (Ti,Mo)C/C and reference samples cp-Ti and Ti-6Al-4V

The comparison of the results of corrosion tests of the (Ti,Mo)C/Ti and TiC/Ti composites produced in the SLM process and reference samples of cp-Ti and Ti-6Al-4V alloy are shown in Figures 11 and 12. The variation in the open circuit potentials (OCP) of the produced composites exposed to artificial saliva solution after polishing is presented in Figure 11.

It is observed from figure 11, which presents the OCP profile of the composites containing 5 and 10 wt % of (Ti,Mo) C/C reinforcement, that the open circuit potentials fluctuate continuously. The exception is observed in case of composites containing 5 and 10 wt % of TiC/C, and 20 wt % of (Ti,Mo) C/C and reference samples of the cp-Ti and Ti-6Al-4V alloy which had a fairly stable OCP profile. The fluctuation of OCP

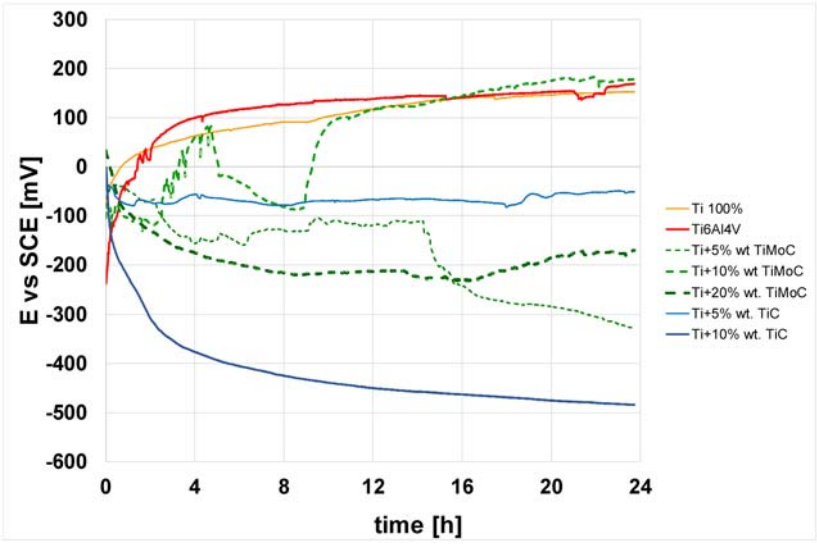

Fig. 11. The variation in the OCP of the composites exposed to artificial saliva solution, pH 6.7 temperature 37°C

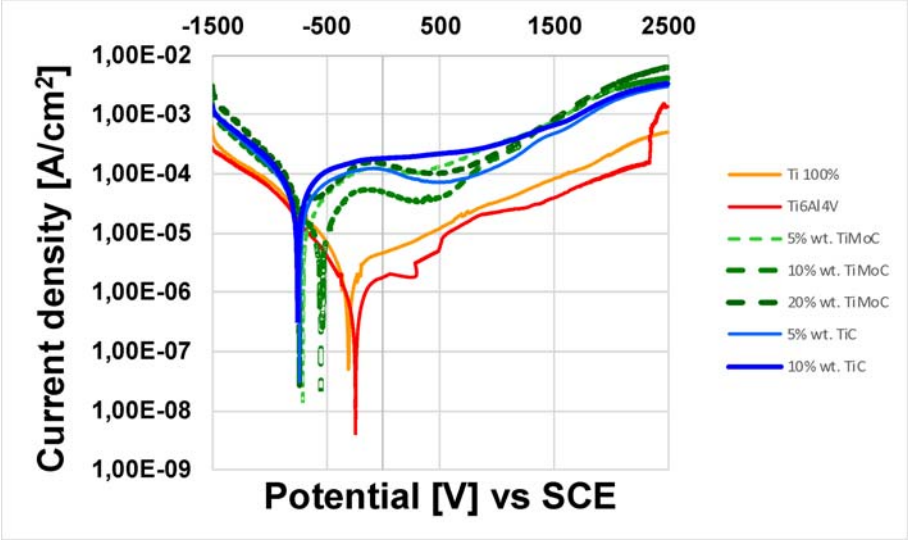

Fig. 12. Comparison of anodic polarization curves of composites (Ti,Mo)C/Ti and TiC/Ti, cp-Ti and Ti-6Al-4V alloy

values in the manner observed in these composites is typical for materials systems undergoing repeated passive film formation and breakdown due to exposure to a corrosive environment. The highest obtained potential values (in descending order) are those of the reference samples of the cp-Ti and Ti-6Al-4V alloy and the composite containing 10 wt % (Ti,Mo)C/C. These values increased in time. In the case of composites containing 10 wt % of TiC/C and 20 wt % of (Ti,Mo)C/C, the potentials monotonously decreased in the first 4 hours, then showed a tendency to stabilize over time . Potential values of composites containing 10 wt % of TiC/C and 5 wt % of (Ti,Mo)C/C showed a decreasing trend in time. Interesting potential changes were observed on the course of the OCP profile for the composite with a 10 wt % of (Ti,Mo) C/C. The potential changed continuously for about 9 hours, and then the potential increased to values comparable with cp-Ti and Ti-6Al-4V alloy, showing an upward trend until the end of the measurements. These results suggest that the oxide layer underwent rebuilding for 9 hours, and then the thermodynamically stable layer with the most favorable protective properties was established. This suggests that the cp-Ti and Ti-6Al-4V alloy and composite containing 10wt % of (Ti,Mo)C/C and also 5 wt % of TiC/C will have the least thermodynamic tendency to corrode in the artificial saliva solution.

The potentiodynamic polarization curves for the composites in artificial saliva solution, pH 6.7 temperature 37°C (Fig. 12) help in analyzing more thoroughly the corrosion behavior of the composites. Figure 12 shows that the composites generally displayed similar polarization curves and passivity characteristics. However, the corrosion potentials (E_{corr}) of the composites were clearly distinct and occurred in the ranges of −0.545 to −0.750 V. Table 3, which presents the corrosion potential (E_{corr}) and corrosion current density (I_{corr}) data of all the composites produced, was obtained from figure 12. On analysis of the composites in this test, it is noted that the corrosive potentials (E_{corr}) and the density of the corrosive current (Icorr) of the composites show a constant tendency of changes in value along with a change in the reinforcement phase. An exception to this rule is the composite with a 10 wt % of (Ti,Mo)C/C. Probably it is connected with lower porosity of this compsite.

In case of pure Ti sintered sample immersed in artificial saliva solution, corrosion potential was at the level of –0.304 V and corrosion current density reached $0.605 \cdot 10^{-6}$ A·cm^{-2}, and in the case of Ti-6Al-4V alloy corrosion potential was at the level of –0.243V and corrosion current density reached $0.203 \cdot 10^{-6}$A·cm^{-2} (Tab. 3). When TiMMCs are immersed in artificial saliva solution, the corrosion potential generally shifts to lower values to-

TABLE 3

Corrosion parameters of the composites exposed to artificial saliva solution, pH 6.7 temperature 37°C

Samples	E_{cor}, [mV]	i_{cor}, [A/cm^2]	R_{pol} [Ω·cm^2]	β_a [mV·dec^{-1}]	β_c [mV·dec^{-1}]
cp-Ti	–304	$0.605 \cdot 10^{-6}$	$51 \cdot 10^3$	32	37
Ti-6Al-4V	–243	$0.203 \cdot 10^{-6}$	$132 \cdot 10^3$	38	37
Ti + 5 wt % (Ti,Mo)C	–706	$3.41 \cdot 10^{-6}$	$4.1 \cdot 10^3$	28	39
Ti + 10 wt % (Ti,Mo)C	–545	$3.48 \cdot 10^{-6}$	$9.89 \cdot 10^3$	35	37
Ti + 20 wt % (Ti,Mo)C	–735	$7.81 \cdot 10^{-6}$	$2.45 \cdot 10^3$	21	21
Ti + 5 wt %TiC	–733	$5.91 \cdot 10^{-6}$	$3.6 \cdot 10^3$	46	41
Ti + 10 wt %TiC	–750	$9.25 \cdot 10^{-6}$	$2.42 \cdot 10^3$	49	51

wards cathodic region. The deterioration of corrosion resistance of a nanocomposite with a content of 20% by weight (Ti,Mo)C/C compared to the other composites containing (Ti,Mo)C/C was probably due to the increase in their porosity. The best corrosion resistance, measured by the relatively higher values of resistance polarization (R_{pol}), characterized the Ti-6Al-4V alloy, pure titanium and composite with a 10 wt % of (Ti,Mo) C/C. Comparing titanium composites, it can be concluded that the addition of molybdenum to TiC increases the resistance of titanium reinforced with titanium carbides.

4. Conclusion

In this study, results of investigation on SLM-processed bulk-form Titanium Metal Matrix NanoComposites reinforced with nc-(Ti,Mo)C and nc-TiC type carbides were presented. The properties of the TiMMNCs were compared with the bulk-form titanium cp-Ti and Ti-6Al-4V alloy. Prior to the SLM processes, nc-(Ti, Mo) C and nc-TiC carbides were surrounded by a carbon network. During sintering, the consolidation of the material took place involving a chemical reaction between the elemental carbon and the titanium matrix to form TiC. In the case of (Ti,Mo) C/Ti composites, the process of diffusion of Mo atoms in the direction of the titanium matrix and the formation of the Ti-Mo alloy took place and additionally the nanocrystalline carbides formed grains of a few micrometers size.

The results of X-ray diffraction tests indicate that in titanium composite samples, Ti and carbide phases exhibits some texture.

The results showed that the hardness of the TiMMNCs increased with increasing carbide content. The composites were characterized by slightly higher values of COF in comparison to cp-Ti and Ti-6Al-4V alloy.

Interesting electrochemical potential changes were observed on the course of the OCP profile for the composite with a 10 wt % of (Ti,Mo)C/C. The potential fluctuated for about 9 hours, and then increased to values comparable with cp-Ti and Ti-6Al-4V alloy, showing an upward trend until the end of the measurements. These results suggest that the oxide layer underwent rebuilding for 9 hours, and then the thermodynamically stable layer with the most favorable protective properties was established. The results of OCP tests suggest that the cp-Ti and Ti-6Al-4V alloy and composite containing 10wt % of (Ti,Mo)C/C and also 5 wt % of TiC/C will have the least thermodynamic tendency to corrode in the artificial saliva solution The best corrosion resistance measured by the relatively higher values of resistance polarization (R_{pol}) characterized the Ti-6Al-4V alloy, pure titanium and composite with a 10 wt % of (Ti,Mo)C/C. Better corrosion resistance of (Ti.Mo)C/Ti composites in the comparison of TiC/Ti composites could be explained: smaller size of carbides crystallites (ca. 12 nm for ca. 40 nm). Additionally, high ratio of molar volumes of MoO_2 to Mo (Pilling-Bedworth coefficient equals 3,45) has a positive effect on sealing the grains and reduces the corrosive attack on the grain boundaries.

REFERENCES

[1] P.I. Brånemark, B.O. Hansson, R. Adell, U. Breine, J. Lindstrom, O. Hallen, A. Ohman, Scand. J. Plast. Reconstr. Surg. Suppl. **16**, 1-132 (1977).

[2] K.J. Anusavice, Phillips' Science of Dental Materials 11th Edition, Saunders; St. Louis, (2003).

[3] R.C. Petersen, Metals; **4**(4), 549-569 (2014).

[4] Y.S. Tian, C.Z. Chen, L.B. Chen, J.H. Liu, T.Q. Lei, J. Mater. Sci. **40**, 4387-4390 (2005).

[5] M. Long, H.J. Rack, Wear **249**, 157-167 (2001).

[6] S. Fouvry, C. Paulin, S. Deyber, Tribol. Int. **42**, 461-474 (2009).

[7] C. Poletti, M. Balog, T. Schubert, V. Liedtke, C. Edtmaier, Compos. Sci. Technol. **68** (9), 2171-2177 (2008).

[8] D.E. Alman, J.A. Hawk, Wear **225-229**, 629-639 (1999).

[9] H.O. Gülsoy, V. Gunay, T. Baykara, Powder Metall. **58** (1), 30-35 (2015).

[10] A.A.M. da Silva, A. Meyer, J.F. dos Santos, C.E.F. Kwietniewski, T.R. Strohaecker, Compos. Sci. Technol. **64**, 1495-1501 (2004).

[11] N. Takahashi, T. Sato, S. Nakatsuka, K. Fujiwara, K. Yokozekii, Titanium metal matrix composite development for commercial aircraft landing gear structure, Proceedings of 28th International Congress of The Aeronautical Sciences 2012, Brisbane, Australia, (2012).

[12] S. Cruz, P. Rey, M. Cabeza, M. Lieblich, P. Merino, Effect of the TiC particle size on the extrusion of 7075 aluminium matrix composite, ECCM16 – proceedings of the 16th European Conference on Composite Materials, Seville, Spain, (2014).

[13] D. Gu, Y-C. Hagedorn, W. Meiners, K. Wissenbach, R. Poprawe, Compos. Sci. Technol. **71**, 1612-1620 (2011).

[14] P.D. Zhou, F. Qiu, H. Wang, Q. Jiang, Acta Metall. Sin. (Engl. Lett.) **27** (5), 798-805 (2014).

[15] Z. Wang, H. Zhang, C. Guo, W. Liu, Z. Yang, X. Sun, Z. Zhang, F. Jiang, J. Mater. Sci. **51** (10), 4996-5007 (2016).

[16] Z.H. Wang, D. Li, D.Y. Geng, S. Ma, W. Liu, Z.D. Zhang, Phys. Stat. Sol. (A) **205** (12), 2919-2923 (2008).

[17] C.I. Sathish, Y. Guo, X. Wang, Y. Tsujimoto, J. Li, S. Zhang, Y. Matsushita, Y. Shi, H. Tian, H. Yang, J. Li, K. Yamaura, J. Solid State Chem. **196**, 579-585 (2012)

[18] V.V. Krainika, A. Lisenkov, V.I. Ivashchenko, V.L. Bekenev, Phys. Stat. Sol. (B) **194**, 575-583 (1996)

[19] J.H. Jang, C-H. Lee, Y-U. Heo, D-W. Suh, Acta Mater. **60**, 208-2017 (2012),

[20] Y. Funakawa, T. Shiozaki, K. Tomita, T. Yamamoto, E. Maeda, ISIJ Int. **44**, 1945-1951 (2004).

[21] O. Kontsevoi, A.J. Freeman, G.B. Olson, Adhesive strength of interfaces between bcc and fcc Fe and transition metal carbides: effect of misfit dislocations on structure and bonding, Proceedings of 30th Annual SRC Meeting, Evanston, USA, (2014).

[22] A. Biedunkiewicz, J. Sol-Gel Sci. Technol. **59**, 448-455 (2011).

[23] Y.K. Kim, J-H. Shim, Y. W. Cho, H-S. Yang, J-K. Park, Int. J. Refract. Met. Hard Mater. **22**, 193-196 (2004).

[24] J-H. Shim, C-S. Oh, D.N. Lee, Metall. Mater. Trans. B, **27**, 955-966 (1996).